THE JOURNAL OF PHYSICAL CHEMISTRY C

ARTICLE

pubs.acs.org/JPCC

Study of Growth Mechanism and Properties of Zinc Indium Sulfide Thin Films Deposited by Atomic Layer Chemical Vapor Deposition over the Entire Range of Composition

Pascal Genevée,* Frédérique Donsanti,* Gilles Renou, and Daniel Lincot

Institut de Recherche et Développement sur l'Energie Photovoltaïque (IRDEP), UMR 7174 EDF−CNRS−Chimie ParisTech, 6, Quai Watier, 78401, Chatou, France

ABSTRACT: In this study, zinc indium sulfide (ZIS) thin films of different compositions ranging from pure In_2S_3 to pure ZnS were synthesized by atomic layer chemical vapor deposition (ALCVD). In situ growth mechanism studies were carried out using the quartz crystal microbalance technique. They evidence preferential surface exchange reactions between indium and zinc ions during ALCVD pulses, which control the overall composition. Optical characterizations indicate a bandgap varying from 2.0 eV with indirect transition for In_2S_3 to 3.6 eV with direct transition for ZnS. As deposited films present good crystallinity toward the two binary compounds which decreases at intermediate compositions. An amorphous phase appears in the material for the In/(In + Zn) ratio in the range 11−73 at % attributed to the conflict between the crystallographic structures of ZnS and In_2S_3. Under thermal annealing treatments, grown films undergo crystallization processes. In particular, the thermal annealing of a sample with In/(In + Zn) ∼ 73 at % leads to the formation of the crystalline phase $ZnIn_2S_4$ with the presence of the crystallized In_2S_3 phase.

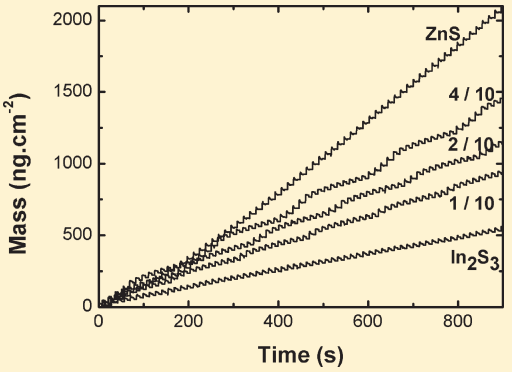

1. INTRODUCTION

As reviewed recently, indium sulfide and zinc sulfide thin films are widely studied as potential layers to replace cadmium sulfide (CdS) layers in copper indium gallium diselenide (CIGS) solar cells[1,2] at the interface between the CIGS inner layers and ZnO based outer layers. These layers are called buffer layers and play a critical role in fixing the final photovoltaic quality of the whole device. In these applications, the optoelectronic properties of the buffer layers are tuned by the introduction of foreign elements, as for instance, oxygen in zinc sulfide giving Zn(O,S) films with a controlled electron affinity for a better matching with the CIGS conduction band edge.[3] In the case of indium sulfide, substitution by aluminum, sodium, and oxygen has been studied.[4−6] However, mixed systems between zinc sulfide and indium sulfide have not been studied extensively up until now. Recent studies report on the use of ZnS/In_2S_3 bilayers.[7] There is thus a great interest to explore completely mixed films since we can expect the possibility of fine-tuning of the electronic properties from those of pure zinc sulfide to pure indium sulfide. In particular, the bandgap from 2 to 3.6 eV and the electron affinity from 3.1 to 4.8 eV could be adapted by using mixed $ZnS−In_2S_3$ films. This is the objective of this study using a very versatile deposition method for composition control which is atomic layer chemical vapor deposition (ALCVD). We can note that the highest efficiencies have been obtained by ALCVD both for the zinc oxysulfide systems and indium sulfide.[8,9]

ALCVD also named atomic layer deposition (ALD) is a thin film deposition method based on sequential, self-limited surface chemical reactions in the gaseous phase which allows an excellent control of the thickness and the composition.[10] Indium sulfide has been first deposited by ALD using indium chloride ($InCl_3$) and hydrogen sulfide (H_2S) at substrate temperatures of 300 and 400 °C.[11] However, in order to prevent thermal degradation, a lower deposition temperature around 150−200 °C is desired to deposit buffer layers in CIGS solar cells; therefore, indium acetylacetonate ($In(acac)_3$) has been used as a precursor for the deposition of indium sulfide at temperatures between 120 and 240 °C[12−14] thanks to a higher vapor pressure than indium chloride. Zinc sulfide films have already been deposited by ALD in the same range of temperature using diethylzinc (DEZ) and H_2S.[3,15−18]

Direct growth of $ZnIn_xS_y$ films by ALD has been carried out over the whole composition range, which has never been done before to our knowledge. The deposition temperature is 200 °C, which is convenient for both In_2S_3 and ZnS systems. First, an in situ study was done using a quartz crystal microbalance (QCM) in order to determine the growth kinetics of the two binary boundary materials (ZnS, In_2S_3) and mixed films. Second, thin films have been deposited on glass substrates. Their optical properties, composition, and crystal structure were investigated and discussed in relation with growth mechanism insights.

Received: April 18, 2011
Revised: July 19, 2011
Published: July 20, 2011

dx.doi.org/10.1021/jp203604j | J. Phys. Chem. C 2011, 115, 17197–17205

2. EXPERIMENTAL PROCEDURE

Thin film depositions have been carried out in a ASM Microchemistry F-120 reactor. The reaction chamber can receive two 5 × 5 cm^2 substrates located face to face at a distance of 1 mm. The source material for zinc was diethylzinc ($Zn(C_2H_5)_2$), DEZ, Optograde provided by Rohm and Haas. The source material for indium was indium acetylacetonate ($In(CH_3COCHCOCH_3)_3$), $In(acac)_3$, (98%) from Alfa Aesar GMBH & Co KG. H_2S (99.5%) from Messer was used as the sulfur source. DEZ and H_2S sources were kept at room temperature while $In(acac)_3$ was heated at 125 °C. The carrying gas was nitrogen with a purity of 99.9999% provided by Messer. The pressure in the reaction chamber was kept in the range 1−5 mbar.

First, an in situ study was done by depositing films on a quartz crystal microbalance (QCM) in order to study the growth kinetics of zinc sulfide, indium sulfide, and mixed films at 200 °C. The QCM is based on an AT cut quartz with a resonance frequency of 5 MHz measured using a Maxtek TM-400 thickness monitor. Quartz crystals are made of fused quartz with a density of 2.2 $g.cm^{-3}$ which were covered with gold layers serving as electrodes and substrate for the growth of the film. The quartz crystal is fixed in the reaction chamber as described in a previous paper.[19] Measurements were done after a stabilization time of a few hours in order to reach a temperature in the reaction chamber as stable as possible (ΔT < 0.2 °C).

Second, films were deposited on borosilicate glass substrates. An annealing of a sample with a composition close to $ZnIn_2S_4$ was done in a tubular furnace at a temperature of 500 °C for 2.5 h under argon atmospheric pressure. The sample was placed in a graphite box with 3 mg of elemental sulfur in order to limit the sulfur losses of the material.

Zinc, indium, and sulfur atomic contents in each film were measured using energy-dispersive X-ray spectroscopy (EDX) on a ZEISS ULTRA 55 SEM FEG with a tilt angle of 70° in order to increase the interaction between the electron beam and the films. Crystal structures were analyzed by grazing incidence X-ray diffraction (GIXRD) which was done using a Bruker D8 Advance (θ/θ) diffractometer with a Göbel mirror attachment at an incident angle of 0.7°. Films thickness were determined using a VEECO DEKTAK 6 M profilometer. Thicknesses are determined after creating steps in the film. They are prepared by masking parts with chemically resistant tape and dipping the film in diluted nitric acid with a mass concentration of 10% at room temperature for 30 s. The uncertainty given for the thickness is a standard deviation of eight measurements taking into account profilometer uncertainty, sharpness of steps, film roughness, and film inhomogeneity. Transmittance and reflectance spectra were obtained using a PerkinElmer lambda 900 spectrophotometer with an integrating sphere.

3. RESULTS

3.1. In Situ Growth Kinetic Study. The deposition of a binary material by ALD is done by exposing the substrate surface to two gas phase reactants sequentially. Each exposure is followed by a nitrogen purge. The succession of these two reactant pulses and their respective purges is called a growth cycle.

Figure 1 gives an example of a growth curve recorded using QCM. The curve with the highest slope is the ZnS growth curve and the curve with the lowest slope is that of In_2S_3. Between these two curves are represented intermediate curves which correspond

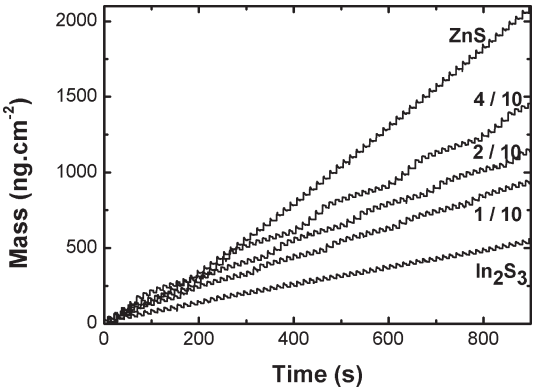

Figure 1. In situ monitoring of thin films deposition using the QCM. A ZnS growth curve is represented at the top and an In_2S_3 growth curve is represented at the bottom. Ratios indicated for intermediate growth curves correspond to the ratios (number of ZnS cycles/number of In_2S_3 cycles).

to In_2S_3−ZnS growth curves with different number of ZnS cycles inserted every 10 In_2S_3 cycles. The more ZnS cycles are inserted, the higher the mean slope is. The insertion of ZnS cycles results in a temporarily increased growth rate of In_2S_3 on the curve.

To observe mass changes during individual pulses, different pulse durations have been studied with a constant purge time of 6 s after each pulse. Growth cycles were repeated a minimum of 30 times and then averaged, after subtraction of the mass uptake from previous cycles, to obtain a more accurate value of the mass deposited. This allows a significant improvement of the precision of mass variations.

Figure 2 shows mass variations during one growth cycle for ZnS and In_2S_3 as a function of DEZ, $In(acac)_3$, and H_2S pulse durations. In these graphs, the first mass increase corresponds to the metal precursor pulse which is DEZ for the growth of ZnS (graphs A and B) and $In(acac)_3$ for the growth of In_2S_3 (graphs C and D). The pulse duration is varied from 0.4 to 1 s in graphs A and C and is fixed to 1 s in graphs B and D. A first 6 s N_2 purge is done right after this pulse. During this purge, strong mass decreases are observed indicating desorption of species. It appears that this desorption reaches a limiting value.

The H_2S pulse starts at the middle of the graph, directly after the first purge, with a duration varying between 0.1 and 1 s in graphs B and D and fixed to 1 s in graphs A and C. The reaction between DEZ adsorbed on the surface and H_2S leads to a mass increase. On the opposite, the reaction between $In(acac)_3$ adsorbed and H_2S leads to a strong mass loss. A second 6 s N_2 purge is done after the H_2S pulse. During this second purge, no mass change is observed.

For both materials, ZnS and In_2S_3, the mass gain per cycle (MGPC) increases with metal precursors and H_2S pulse durations until surface saturation is reached. The final value of each curve corresponds to the MGPC. The maximum value of MGPC measured is around 42.6 ng cm^{-2} for ZnS and 12.6 ng cm^{-2} for In_2S_3. From these values, one can calculate the zinc and indium molar deposition rates per surface unit n_{Zn} and n_{In} using the following equations: $n_{Zn} = MGPC_{ZnS}/M(ZnS)$ and $n_{In} = 2\{MGPC_{In_2S_3}/M(In_2S_3)\}$, where $M(ZnS)$ and $M(In_2S_3)$ are, respectively, the molar masses for zinc sulfide and indium sulfide. The values obtained after calculation are $n_{Zn} = 4.37 \times 10^{-1}$ nmol cm^{-2} $cycle^{-1}$ and $n_{In} = 7.73 \times 10^{-2}$ nmol cm^{-2} $cycle^{-1}$. We conclude that the molar deposition rate of zinc is about 6 times higher than the one of indium.

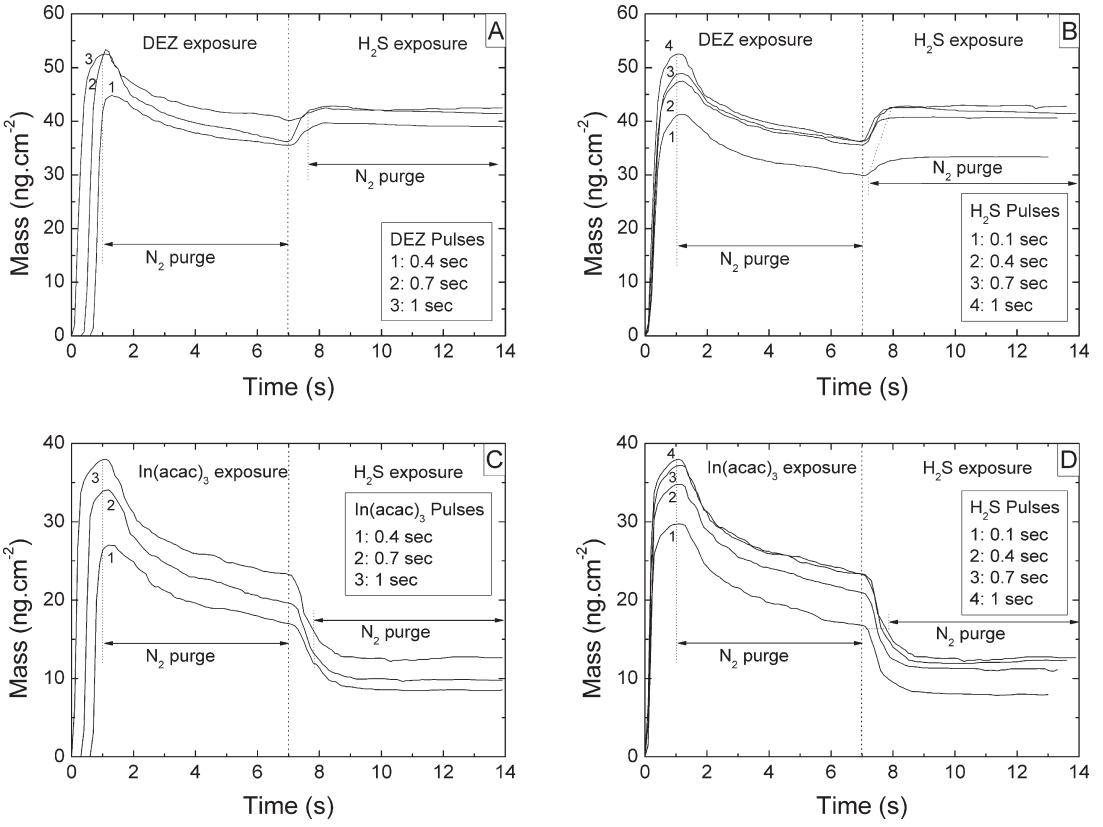

Figure 2. In situ growth kinetics results for pure indium sulfide and zinc sulfide layers as a function of pulse parameters at 200 °C. (A,B) Mass variations for ZnS ALD at 200 °C: (A) 1 s H_2S pulse time and variable DEZ pulse times and (B) 1 s DEZ pulse time and variable H_2S pulse times. (C,D) Mass variations for In_2S_3 ALD at 200 °C: (C) 1 s H_2S pulse time and variable $In(acac)_3$ pulse times, (D) 1 s $In(acac)_3$ pulse time and variable H_2S pulse times.

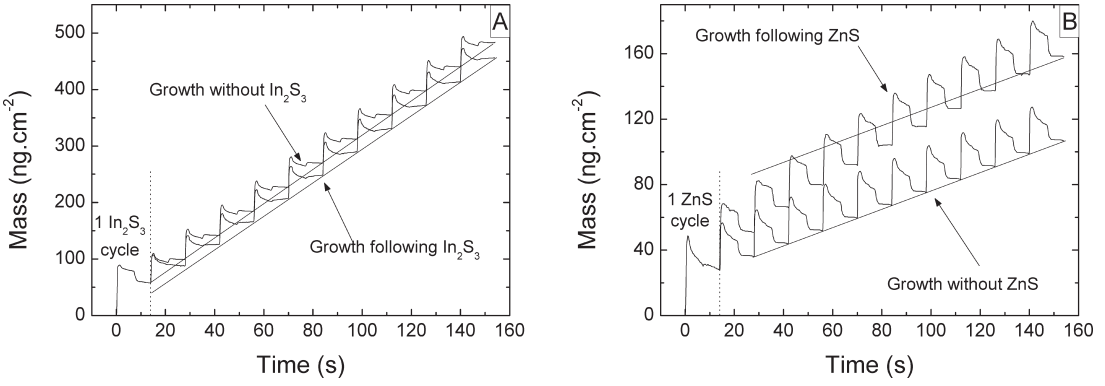

Figure 3. Effect of the introduction of a foreign cycle on the growth kinetics of In_2S_3 and ZnS at $T = 200$ °C. (A) 1 In_2S_3 cycle followed by 10 ZnS cycles and a reference ZnS growth curve, (B) 1 ZnS cycle followed by 10 In_2S_3 cycles and a reference In_2S_3 growth curve. Straight lines are guides for the eye and correspond to the average slope of the reference curve.

The QCM was also used to study the effect of single cycle insertion of In_2S_3 in ZnS growth cycles and ZnS in In_2S_3 growth cycles. Each pulse durations were set to 1 s and purge durations were set to 6 s. The following sequences were studied: (i) 1 In_2S_3 cycle followed by 10 ZnS cycles and (ii) 1 ZnS cycle followed by 10 In_2S_3 cycles. Each sequence is repeated 8 times and averaged.

Figure 3A shows mass gains during the growth of ZnS cycles following 1 In_2S_3 cycle and a reference averaged curve of the growth of ZnS without In_2S_3. Figure 3B shows mass gains during the growth of In_2S_3 cycles following 1 cycle of ZnS and a reference averaged curve. Two opposite phenomena appear in these curves. When ZnS is deposited after In_2S_3, the growth rate is lower than the reference one, whereas if In_2S_3 is deposited after ZnS, the growth rate is higher than the reference one. After a few cycles, the MGPC of both cycles come back to the average value previously determined. It takes 1 to 2 cycles in the case of ZnS, but in the case of In_2S_3 the value of MGPC of the reference curve is only reached after about 10 cycles.

3.2. Film Characterization. For practical reasons, growth cycles durations during the synthesis of samples have been shortened in order to get films with a thickness of about 100 nm in a reasonable time. Precursor pulse durations were

dx.doi.org/10.1021/jp203604j |J. Phys. Chem. C 2011, 115, 17197–17205

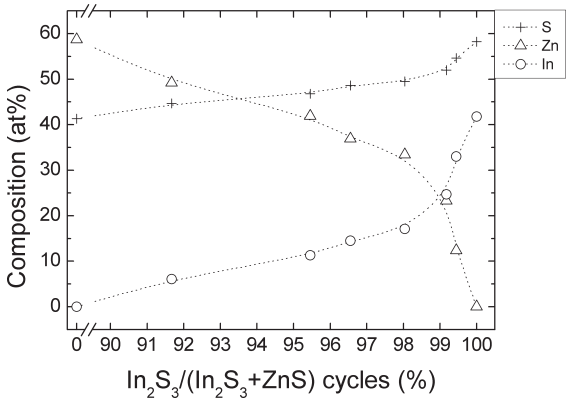

Figure 4. Composition of films as a function of the $In_2S_3/(ZnS + In_2S_3)$ cycles ratio. The dotted line is a guide for the eye.

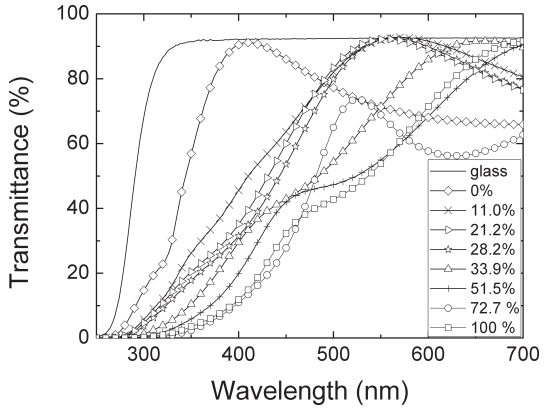

Figure 6. Variation of transmittance toward sample composition. Corresponding ratios In/(In + Zn) are indicated in the legend.

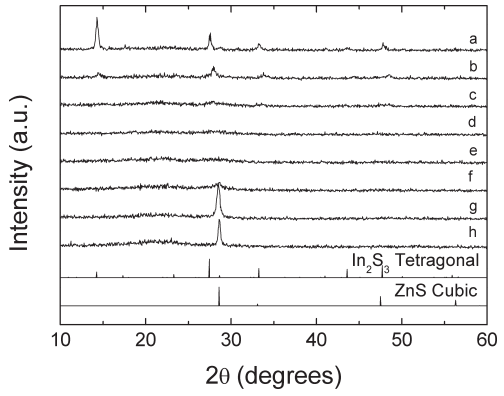

Figure 5. Diffraction patterns for samples with various indium contents. In/(In + Zn) = (a) 100 at %, (b) 72.7 at %, (c) 51.5 at %, (d) 33.9 at %, (e) 28.2 at %, (f) 21.2 at %, (g) 11.0 at %, and (h) 0 at %. The In_2S_3 and ZnS diffraction patterns are taken from databases JCPDS 00-025-0390 and JCPDS 00-005-0566.

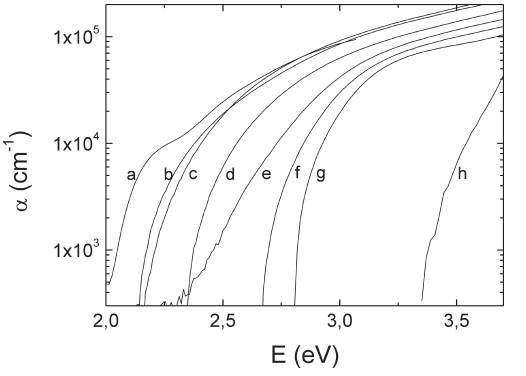

Figure 7. Variation of the absorption coefficient as a function of photon energy for thin films of $ZnIn_xS_y$ with different compositions. In/(In + Zn) = (a) 100 at %, (b) 72.7 at %, (c) 51.5 at %, (d) 33.9 at %, (e) 28.2 at %, (f) 21.2 at %, (g) 11.0 at %, and (h) 0 at %.

kept to 1 s, purge durations following DEZ and $In(acac)_3$ pulses were set to 3 s, and purge durations following H_2S pulses were set to 2 s. These values have been determined from mass variation observed during the in situ study. Precursor pulses have been chosen long enough to reach surface saturation. Purges after metal precursor sequences are longer than H_2S ones to reduce the influence of mass variations due to desorption. We have synthesized different samples with different In_2S_3/ZnS cycles ratios. We have calculated that the zinc molar deposition rate is about 6 times higher than the indium one. To reach intermediate composition, we use growth sequences with more In_2S_3 cycles than ZnS. Sequences used for films deposition were composed of 1 ZnS cycle and the following numbers of In_2S_3 cycles: {0, 11, 21, 28, 50, 120, 180}. At last, a film of pure In_2S_3 was also synthesized.

Figure 4 represents zinc, indium, and sulfur contents in the films determined by EDX as a function of the $In_2S_3/(ZnS + In_2S_3)$ cycles ratio. We note that ZnS films grown under these conditions are not purely stoichiometric. The ratio S/Zn is 0.70 in place of 1. In the case of In_2S_3, this sulfur deficiency is less important and the S/In ratio is 1.39 instead of 1.5. A previous study of the growth of In_2S_3 at 150 °C, in which a S/In ratio of 1.42 was found, revealed the presence of about 5 at % of carbon in the bulk using XPS measurements after argon sputtering.[12] Another ZnS film was deposited with longer pulse durations of 3 s and purge durations of 6 s. Under these conditions, the S/Zn ratio measured was exactly 1.00. Additional characterizations are needed to determine if other elements appear in the case of ZnS films grown with shortened cycles parameters.

GIXRD have been performed to study the crystal structure of the films as well as their crystallinity. Figure 5 represents XRD patterns for the different compositions. We can see that both In_2S_3 and ZnS films are well crystallized while mixed films exhibit lower peak intensities with a minimum for In/(In + Zn) between 28.2 at % and 51.5 at %.

Transmittance and reflectance spectra were recorded on films deposited on borosilicate glass substrates. In Figure 6, the different transmission spectra including the glass substrate are presented. We observe a shift in the absorption edge from the long wavelength for zinc poor layers to the short wavelength for the zinc rich layers indicating a relation between the apparent bandgap of the material and its composition. The absorption coefficient α was deduced from transmittance and reflectance spectra using the formula $\alpha = -(1/t)\ln\{T/(1 - R)\}$, where t is the film thickness, T the transmittance, and R the reflectance.

Figure 7 represents the absorption coefficient as a function of photon energy with a semilogarithmic scale. On this graph we can see the displacement of the absorption edge from the ZnS curve to the In_2S_3 curve. The sample corresponding to In/(In + Zn) = 28.2% shows an absorption edge tending to a straight line, which

Table 1. Film Properties As a Function of the Ratio In_2S_3/ZnS cycles

In_2S_3/(In_2S_3 + ZnS) cycles	number of cycles	film thickness (nm)	growth rate (Å cycle^{-1})	In/(In + Zn) (at %)	optical bandgap (eV)	optical transition
1/1	5000	161 ± 6	0.32	100	2.05 ± 0.05	indirect
180/181	6291	183 ± 13	0.29	72.7	2.10 ± 0.05	indirect
120/121	4810	129 ± 18	0.27	51.5	2.15 ± 0.05	indirect
50/51	4080	137 ± 7	0.34	33.9	2.30 ± 0.05	indirect
28/29	3364	120 ± 3	0.36	28.2	2.30 ± 0.05	amorphous
21/22	3014	131 ± 20	0.43	21.2	2.65 ± 0.05	indirect
11/12	2232	135 ± 12	0.60	11.0	3.05 ± 0.05	direct
0/1	745	95 ± 8	1.28	0	3.65 ± 0.05	direct

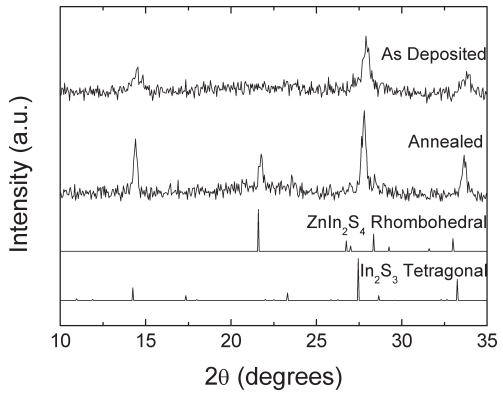

Figure 8. XRD patterns of the sample with In/(In + Zn) = 72.7 at % before and after annealing. The $ZnIn_2S_4$ reference diffraction pattern is taken from the database JCPDS 00-049-1562.

is typical of an amorphous film. This confirms the result obtained with GIXRD.

Table 1 sums up the different films properties including the values of bandgaps determined. The types of optical transitions considered for this determination have been chosen comparing $[\alpha(E)E]^2$ vs E, $[\alpha(E)E]^{0.5}$ vs E, or $\log[\alpha(E)]$ vs E, where E is the photon energy. One should find $\alpha(E)$ proportional to $(E - Eg)^{0.5}/E$ in the case of a direct optical transition,[20] $\alpha(E)$ proportional to $(E - Eg)^2/E$ in the case of an indirect optical transition,[20] and $\alpha(E)$ proportional to $\exp(E - E_0)$ in the case of an optical transition between band tails in an amorphous material.[21]

The sample with a ratio In/(In + Zn) = 72.7 at % is the closest to the one of $ZnIn_2S_4$, which is In/(In + Zn) = 66.7 at %. Nitsche[22] had shown in his study that the phase $ZnIn_2S_4$ can be obtained for an indium content from 66.7 at % to 75 at %, so this sample may allow this phase formation. On the corresponding XRD pattern of the Figure 5, only In_2S_3 diffraction peaks appear, so thermal annealing of the sample was performed to reach the rhombohedral phase formation. Deposited and annealed samples present the same composition and the same optical properties. Figure 8 shows their XRD patterns. The annealed sample presents a diffraction peak at an angle of 21.8°, which does not appear in the case of the as deposited sample.

4. DISCUSSION

During the metal precursor pulses, in Figure 2, the mass strongly increases indicating the adsorption of molecules. The classical mechanism considered for the precursor adsorption is a reaction leading to the creation of a bond between the metal atom from the molecule and one sulfur atom from the substrate:

$$ML_n + SH^* \rightarrow LH + SML_{n-1}^*$$

where the asterisks indicate the surface species, M stands for metal, and L stands for ligand. We consider a second possible adsorption mechanism involving electrostatic interactions between DEZ or $In(acac)_3$ molecules and thiol groups:

$$ML_n + SH^* \rightarrow SH - ML_n^*$$

This second mechanism creates weak van der Waals bonds while the first mechanism creates strong covalent bonds.

During the precursor purge, a mass loss is observed indicating desorption of species. This mass loss may be caused by the desorption of another ligand but also by the rapid desorption of DEZ molecules weakly linked with the substrate.

In the case of ZnS, the H_2S exposure leads to a mass increase. One can determine reaction equations from mass variations. In Figure 2B curve 4, the maximum mass adsorbed during the DEZ pulse is 52.5 ng cm^{-2}. This mass decreases down to 36.2 ng cm^{-2} after the first N_2 purge and finally stabilizes at 42.5 ng cm^{-2} after H_2S exposure. If we only consider the first adsorption mechanism, the final mass should be equal to

$$52.5\frac{M(\mathrm{ZnS})}{M(\mathrm{DEZ}) - M(\mathrm{C_2H_6})} = 52.5\frac{97.44}{93.43} \approx 54.8 \text{ ng cm}^{-2}$$

referring to the partial reactions:

$$Zn(C_2H_5) + SH^* \rightarrow SZnC_2H_5^* + C_2H_6 \quad \text{(DEZ adsorption)}$$

$$SZnC_2H_5^* + SH^* \rightarrow SZnS^* + C_2H_6 \quad \text{(ligand desorption)}$$

$$SZnS^* + H_2S \rightarrow SZnSH^* + SH^* \quad \text{(ZnS formation)}$$

If we consider only the second adsorption mechanism, the final mass should be equal to

$$36.2\frac{M(\mathrm{ZnS})}{M(\mathrm{DEZ})} = 36.2\frac{97.44}{124.10} \approx 28.4 \text{ ng cm}^{-2}$$

referring to the two half reactions:

$$Zn(C_2H_5)_2 + SH^* \rightarrow SH - Zn(C_2H_5)_2^*$$
(DEZ adsorbed at the end of the first purge)

$$SHZn(C_2H_5)_2^* + H_2S \rightarrow SZnSH^* + 2C_2H_6$$
(ZnS formation)

The first hypothesis leads to a final mass higher than the real one while the second hypothesis leads to a final mass lower than the

dx.doi.org/10.1021/jp203604j |J. Phys. Chem. C 2011, 115, 17197–17205

real one. Thus, a suitable model would imply the contribution of both mechanisms.

In the case of In_2S_3 cycles, the mass loss is assumed to be caused by the replacement of acac groups by sulfur atoms which are lighter. The same reasoning as for ZnS can be applied showing that both mechanisms should also be considered to agree with the MGPC measured.

On Figure 2B,D, we note an increase of the mass uptake during the DEZ and $In(acac)_3$ pulses for longer H_2S pulses. This increase of mass uptake is resulting from a highest density of adsorption sites on the surface. In both adsorption mechanisms considered, adsorption sites are thiol groups which are created during H_2S pulses. As long as surface saturation is not reached, an increase of H_2S pulses length leads to a higher thiol group coverage and thus a higher density of adsorption sites.

Figure 2A shows that for a constant H_2S pulse duration of 1s, the MGPC and the mass adsorbed during the DEZ pulse increase with the DEZ pulse duration. For DEZ pulse durations longer than 0.5 s, the MGPC does not increase. This indicates that the reaction is self-limiting. When saturation is reached, the MGPC is about 42.6 ng cm^{-2}. Assuming a film density of 4.09 g cm^{-3}, we expect at the end of a growth cycle a thickness increase of 1.04 Å. Considering an atomic layer thickness of about 3.12 Å, which is the case for a zinc blend phase oriented with the crystallographic direction [111] perpendicular to the subtract, one growth cycle adds $^1/_3$ of a theoretical atomic layer. This value of thickness per growth cycle is limited by the steric hindrance of DEZ. The thickness increase per cycle of 1.04 Å $cycle^{-1}$ found using the QCM is lower than the value of 1.28 Å $cycle^{-1}$ found using the value obtained with the profilometer. This difference can be explained by a lower density of the film, changes in purge durations between the in-situ study and films growth or a slight temperature drift during QCM experiments which would induce a parasitic frequency change of the quartz crystal. In other reports on ZnS grown at 200 °C, growth rates of 0.7 Å $cycle^{-1}$ and 1.4 Å $cycle^{-1}$ are found.[15,17] The study of Stuyven et al. who reported the higher growth rate was done with very short purge durations of 0.5 s. Under these conditions, the samples obtained were not homogeneous which is attributed to an insufficient DEZ dosing. The growth rate was reported to decrease strongly from 1 Å $cycle^{-1}$ to 0.2 Å $cycle^{-1}$ when the DEZ purge time was increased from 0.3 to 0.7 s. This could indicate that the high growth rate observed is caused by an insufficient purge duration leading to a chemical vapor deposition (CVD) growth mechanism, which would explain the film inhomogeneity. The same assertion was done by Bakke et al. who found that a purge of 4 s following the DEZ pulse is required to avoid CVD.[18]

On the one hand, it can be observed, on Figure 2D, that the MGPC of In_2S_3 increases with H_2S pulse durations and does not change for H_2S exposure over 0.7 s for which duration, surface saturation may be reached. On the other hand, Figure 2C shows that the increase of $In(acac)_3$ pulse duration from 0.7 to 1 s induces a noticeable increase of MGPC, so this indicates that surface saturation during $In(acac)_3$ exposure is not obtained yet after 1 s of exposure. In_2S_3 films show various crystallographic orientations. A weighted average of the thicknesses of an atomic layer in these orientations gives a value of about 2.9 Å. The density of indium sulfide is taken to 4.9 g cm^{-3} as reported in the literature.[23] The maximum MGPC measured is 12.6 ng cm^{-2}, which corresponds to a thickness of 0.25 Å or about $^1/_{12}$ of a theoretical atomic layer. In this case, the size of "acac" groups leads to a strong steric hindrance which limits the MGPC. The thickness increase found using the QCM is lower than the value of 0.32 Å $cycle^{-1}$ found using the value obtained with the profilometer. The same hypotheses as those for the ZnS growth can be considered. The difference of material density is one of the most consistent hypotheses. The value of material density can be recalculated from lattice parameters of the reference diffraction pattern JCPDS 00-25-0390. This calculation gives a density of 4.61 g cm^{-3}. In the study on the deposition of In_2S_3 at 150 °C, Sarkar et al. measured a low film density of about 4.31 g cm^{-3} by X-ray reflectivity,[12] which could be caused by the carbon content of the film.

The mass decrease observed during the $In(acac)_3$ purge was also observed in the QCM study of Sarkar et al.[12] in which purge durations were set to 30 s. This mass decrease was not found in the study of Donsanti et al.[13] in which purge durations were set to 0.5 s. This short purge duration prevents the desorption of species and explains the higher growth rate of 0.6 Å $cycle^{-1}$ measured.

The in situ study of mixed films presented in Figure 3 shows that ZnS seems to grow slower when it follows an In_2S_3 cycle and at the opposite, In_2S_3 seems to grow more rapidly when it follows a ZnS cycle. One explanation for this phenomena could be that reactions occur between DEZ and In_2S_3 and between $In(acac)_3$ and ZnS in addition to the classical chemisorption of metal precursors. The equations of these reactions are

$$3DEZ + In_2S_3* \rightarrow 3ZnS* + 2In(C_2H_5)_3 \quad (1)$$

and

$$2In(acac)_3 + 3ZnS* \rightarrow In_2S_3* + 3Zn(acac)_2 \quad (2)$$

3 Zn atoms are lighter than 2 In ones, so when an In_2S_3 surface is exposed to a DEZ pulse, which is in the case in eq 1, a mass decrease should occur and compensate the mass increase due to DEZ chemisorption so the film seems to grow slower. In the case of a ZnS surface exposed to $In(acac)_3$, like in eq 2, a mass increase should be observed so the film seems to grow more rapidly. The same mechanism was observed during the growth of Zn(O,S) films using DEZ, H_2O and H_2S.[24] In that case, oxygen atoms of ZnO layers were replaced with sulfur atoms during the H_2S pulse. It was found that the equivalent of two ZnO cycles were replaced by ZnS during one ZnS cycle.

If we consider that this mechanism is the only one responsible for changes in MGPCs when mixed films are grown, one can calculate the quantities of elements exchanged. This calculation is done on the sequence constituted by 1 ZnS cycle and 10 In_2S_3 cycles. This sequence is close to the one of the sample with $In_2S_3/(In_2S_3 + ZnS)$ cycles = 11/12. Thus, the film In/(In + Zn) ratio on the QCM should be close to the value of 11.0% measured by EDX on this sample.

First of all, we note from Figure 2 that the average value of MGPC during a typical ZnS cycle is about 42 ng cm^{-2}. This can be compared with the value of MGPC during a ZnS cycle surrounded by In_2S_3 cycles; we note from Figure 3B a value of about 28 ng cm^{-2}. The mass difference obtained is called $\Delta m1 = -14$ ng cm^{-2}. According to our hypothesis, this mass difference $\Delta m1$ between these MGPCs is only attributed to the reaction 1. This infers $\Delta m1 = \{3M(ZnS) - M(In_2S_3)\}n_{subs1}$, where n_{subs1} is the number of moles per square centimeter of In_2S_3 replaced by 3 ZnS.

Then, we note from Figure 3B the mass difference at the end of the sequence between the two curves. This mass difference called $\Delta m2 = +152$ ng cm^{-2} is resulting from the presence of ZnS on the surface at the beginning of the In_2S_3 growth. According to our hypothesis, this mass difference is attributed to the reaction in eq 2. This infers $\Delta m2 = \{^1/_3M(In_2S_3) - M(ZnS)\}n_{subs2}$, where

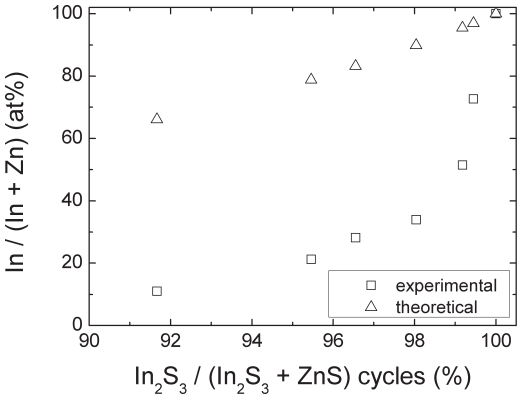

Figure 9. Experimental evidence of a predominant substitution mechanism during the film growth. Triangles represent the theoretical composition of the film calculated considering no specific mechanism. Squares represent experimental points measured by EDX.

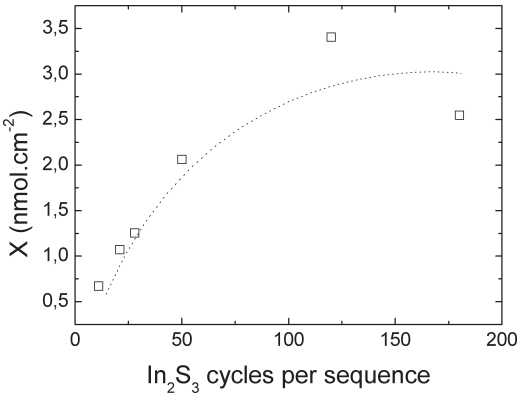

Figure 10. Influence of the number of In_2S_3 cycles per sequence on the quantity of indium atoms replaced during the ZnS cycle. The dotted line is a guide for the eye.

n_{subs2} is the number of moles per square centimeter of ZnS replaced by $^1/_3$ of In_2S_3.

The quantities of indium and zinc deposited per sequence are $n(\mathrm{In}) = 10n_{\mathrm{In}} + \{(^2/_3 n_{subs2}) - 2n_{subs1}\}$ and $n(\mathrm{Zn}) = 1n_{\mathrm{Zn}} - n_{subs2} + 3n_{subs1}$, where n_{Zn} and n_{In} are the zinc and indium molar deposition rates defined previously. One can calculate from these data the ratio $(\mathrm{In}/(\mathrm{In} + \mathrm{Zn})) = \{n(\mathrm{In})\}/\{n(\mathrm{In}) + n(\mathrm{Zn})\} \approx 82\%$. The ratio obtained is very far from the ratio of 11.0% expected from the EDX measurement.

This calculation indicates that substitution mechanisms are not sufficient to explain the modification of the growth rate. During the growth of different materials, the sample surface may change as a function of the material structure, the precursors used, pulses, purge durations, and deposition temperature. All these factors influence the surface roughness and its coverage by thiol groups at the end of cycles which change the density of activated reaction sites. In our case, we assume that the density of reaction sites at the end of ZnS cycles is higher than at the end of In_2S_3 cycles. This can explain why ZnS grows faster after a ZnS cycle than after an In_2S_3 cycle and why In_2S_3 grows also faster after a ZnS cycle than after an In_2S_3 cycle.

Supplementary analysis, like Fourier transform infrared spectroscopy, can be considered in the future to expand on this last hypothesis. However, it is possible to confirm that substitution mechanisms occur by comparing the expected sample composition determined without taking into account any particular mechanism and the real sample composition measured by EDX. We set $N_{In_2S_3}$ as the number of In_2S_3 cycles per sequences while the number of ZnS cycles remains $N_{ZnS} = 1$. The expected composition is given by

$$\frac{\mathrm{In}}{\mathrm{In} + \mathrm{Zn}} = \frac{N_{In_2S_3} n_{\mathrm{In}}}{N_{In_2S_3} n_{\mathrm{In}} + n_{\mathrm{Zn}}}$$

Figure 9 represents this expected composition and the real one as a function of the ratio of In_2S_3 cycles to the total number of cycles, which is simply $(N_{In_2S_3})/(N_{In_2S_3} + 1)$. On this figure, the real curve is clearly lower than expected which indicates that films are more zinc rich than expected. This implies that substitution mechanisms occur and that reaction 1 is the predominant one. Therefore, the highest density of reaction sites after a ZnS cycle explains why the increased growth rate of In_2S_3 is not linked to a substitution mechanism.

It is possible to assess quantitatively the amount of indium replaced by zinc atoms in films using molar deposition rates determined previously and films compositions. We set X as the quantity of indium atoms replaced during a sequence. One can write

$$\frac{\mathrm{In}}{\mathrm{In} + \mathrm{Zn}} = \frac{N_{In_2S_3} n_{\mathrm{In}} - X}{N_{In_2S_3} n_{\mathrm{In}} - X + n_{\mathrm{Zn}} + \frac{3}{2} X}$$

X can be written

$$X = \frac{n_{\mathrm{In}} - (N_{In_2S_3} n_{\mathrm{In}} + n_{\mathrm{Zn}}) \dfrac{\mathrm{In}}{\mathrm{In} + \mathrm{Zn}}}{1 + \dfrac{1}{2} \dfrac{\mathrm{In}}{\mathrm{In} + \mathrm{Zn}}}$$

Figure 10 shows the results of this calculation. It appears that the quantity of replaced indium atoms is not constant as a function of the number of In_2S_3 cycles per sequence. It increases as a function of the number of In_2S_3 cycles per sequence and stabilizes to about 3 nmol cm^{-2}. The more In_2S_3 cycles per sequence is, the less sequences are done during a film growth to reach an equivalent thickness. Fewer sequences lead to samples more dependent on the first cycles during which occurs the nucleation period and on the last cycles which suffer from surface modification due to air exposure. Indeed, surface exposure to air may imply a superficial oxidation and carbon contamination. These phenomena are responsible for increased composition dispersion for such thin samples.

Optical bandgaps found for In_2S_3 and ZnS are similar to those found in the literature for thin films deposited by ALD.[14,3] In the case of In_2S_3 films, previous studies considered a direct transition, like in bulk material, and estimated the bandgap to about 2.8 eV attributed to a quantum confinement effect.[9,13] In all cases, optical properties determined indicate that indium sulfide thin films deposited by ALD exhibit a lower light absorption than bulk material. Films of intermediate composition present a bandgap varying between the band gaps of the two boundary materials. We note that the variation of bandgap is not linear toward the composition variation. The insertion of zinc in indium sulfide modifies its optical properties very slightly while the insertion of indium in zinc sulfide rapidly decreases its bandgap.

The XRD study (Figure 5) shows the transition between the tetragonal structure of In_2S_3 and the cubic structure of ZnS. We observe that the zinc enrichment of In_2S_3 induces a shift of diffraction peaks to the high angles whereas when indium is added in ZnS films diffraction peaks are shifted to the low angles.

Table 2. Position of Peaks and Determination of Lattice Parameters for Zinc Poor In_2S_3 and Indium Poor ZnS

$In_2S_3/(In_2S_3 + ZnS)$ cycles	2θ (deg) (111)	d_{111} (Å)	a (Å)
0/1	28.633	3.115	5.396 ± 0.002
11/12	28.515	3.128	5.418 ± 0.002
21/22	28.482	3.131	5.424 ± 0.015

$In_2S_3/(In_2S_3 + ZnS)$ cycles	2θ (deg) (0012)	d_{0012} (Å)	c (Å)	2θ (°) (103)	d_{103} (Å)	a (Å)
1/1	33.300	2.688	32.262 ± 0.030	14.321	6.180	7.552 ± 0.006
180/181	33.878	2.644	31.727 ± 0.083	14.501	6.104	7.474 ± 0.027

Lattice parameters have been calculated for layers weakly mixed where diffraction peaks are measurable. The diffraction peaks corresponding to (111) planes were used for the calculation of ZnS lattice parameters while peaks corresponding to (0012) and (103) planes were used for In_2S_3 lattice parameters. Results of the calculations are reported in the Table 2.

The lattice parameter of pure ZnS is about 5.396 Å, which is close to the value of 5.406 Å given for the standard diffraction pattern. The addition of indium in the film increases this parameter up to 5.424 Å for In/(In + Zn) = 21.2%. This may indicate that a part of indium is introduced in ZnS grains which lead to the formation of a substitutional solid solution ZnS(In). This is consistent with the difference of ionic radii between Zn^{2+} and In^{3+} which are $r_{Zn^{2+}} = 0.74$ Å and $r_{In^{3+}} = 0.81$ Å.[25] Lattice parameters a and c for pure In_2S_3 were determined as $a = 7.552$ Å and $c = 32.262$ Å. The standard diffraction pattern gives lattice parameters $a = 7.619$ Å and $c = 32.329$ Å, which are higher than those found in our films. In another paper, narrower lattice parameters were also calculated for nanocrystalline In_2S_3 with crystallite sizes between 7.7 and 15.6 nm.[26] A small grain size involving a compressive strain can be an explanation for these smaller lattice parameters. The addition of zinc in the film decreases lattice parameters, contrary to the addition of indium to ZnS, which may indicate the formation of a substitutional solid solution In_2S_3(Zn).

A second effect of the mixing is a decrease of diffraction peaks intensity which entirely disappear for In/(In + Zn) between 28.2 at % and 33.9 at %. The formation of this amorphous phase can be attributed to the conflict between the two crystallographic structures.

In Figure 8, XRD patterns of the sample with In/(In + Zn) = 72.7 at % before and after annealing are compared. We observe that diffraction peaks are higher after annealing, and we observe a new peak at $2\theta = 21.8°$, which is consistent with the main peak (009) of the phase $ZnIn_2S_4$ considering the reference powder diffraction pattern. This points up the metamorphic property of mixed films and confirms that deposition conditions do not allow the direct formation of the intermediate phase $ZnIn_2S_4$.

5. CONCLUSIONS

The deposition of $ZnIn_xS_y$ films over the entire range of composition has been carried out by ALCVD. The in situ growth study using the QCM allowed us to find adequate growth conditions leading to self-limited reactions. This in situ study gives information about the growth kinetics of mixed films and pointed up the presence of substitution mechanisms. This observation was confirmed by EDX measurements done on samples of different composition. However, this mechanism does not totally explain the growth behavior. An additional effect due to a modification of the adsorption behavior of precursors as a function of the surface properties, via the density of adsorption sites, should allow a better description of this behavior. Films deposited on borosilicate glass substrates showed variable absorption properties linked to different band structures. The possibility to obtain a tunable bandgap in the wide range [2.0 eV; 3.6 eV] when it is linked with a tunable electron affinity is interesting to manage electronic band alignments in optoelectronic devices like solar cells. For these reasons, this material should be a good candidate to replace CdS as buffer in CIGS solar cells. Deposited single films present good crystallinity toward the two binary compounds, which decreases at intermediate compositions. An amorphous like material is formed at the composition In/(In + Zn) = 28 at % attributed to the conflict between the two crystallographic structures. Grown films may be polymorphic. In particular, the thermal annealing of a sample with In/(In + Zn) ~ 73 at % led to the formation of the crystalline phase $ZnIn_2S_4$ with the presence of a crystallized In_2S_3 phase. The use of $ZnIn_xS_y$ layers in CIGS solar cells will be investigated in a further study to see if this mixed material allows a real performance improvement of the solar cells.

AUTHOR INFORMATION

Corresponding Author

*Pascal Genevée: phone, + 33 1 30 87 86 90; fax, + 33 1 30 87 85 65; e-mail, pascal-genevee@chimie-paristech.fr. Frédérique Donsanti: phone, + 33 1 30 87 77 55; fax, + 33 1 30 87 85 65; e-mail, Frederique.donsanti@edf.fr.

REFERENCES

(1) Naghavi, N.; Abou-Ras, D.; Allsop, N.; Barreau, N.; Bücheler, S.; Ennaoui, A.; Fischer, C.; Guillen, C.; Hariskos, D.; Herrero, J.; Klenk, R.; Kushiya, K.; Lincot, D.; Menner, R.; Nakada, T.; Platzer-Björkman, C.; Spiering, S.; Tiwari, A.; Törndahl, T. *Prog. Photovolt: Res. Appl.* **2010**, *18*, 411–433.

(2) Barreau, N. *Solar Energy* **2009**, *83*, 363–371.

(3) Platzer-Björkman, C.; Törndahl, T.; Abou-Ras, D.; Malmström, J.; Kessler, J.; Stolt, L. *J. Appl. Phys.* **2006**, *100*, 044506.

(4) Barreau, N. *Thin Solid Films* **2003**, *431−432*, 326–329.

(5) Barreau, N.; Marsillac, S.; Albertini, D.; Bernede, J. C. *Thin Solid Films* **2002**, *403−404*, 331–334.

(6) Couzinié-Devy, F.; Arzel, L.; Barreau, N.; Guillot-Deudon, C.; Harel, S.; Lafond, A.; Kessler, J. *J. Cryst. Growth* **2010**, *312*, 502–506.

(7) Allsop, N.; Camus, C.; Hansel, A.; Gledhill, S.; Lauermann, I.; Luxsteiner, M.; Fischer, C. *Thin Solid Films* **2007**, *515*, 6068–6072.

(8) Platzer-Björkman, C.; Hultqvist, A.; Pettersson, J.; Törndahl, T. *Mater. Res. Soc. Symp. Proc.* **2010**, *7603*, pp 76030F−76030F-9.

(9) Naghavi, N.; Spiering, S.; Powalla, M.; Cavana, B.; Lincot, D. *Prog. Photovolt: Res. Appl.* **2003**, *11*, 437–443.

(10) Suntola, T. *Thin Solid Films* **1992**, *216*, 84–89.

(11) Asikainen, T.; Ritala, M.; Leskela, M. *Appl. Surf. Sci.* **1994**, *82−83*, 122–125.

(12) Sarkar, S. K.; Kim, J. Y.; Goldstein, D. N.; Neale, N. R.; Zhu, K.; Elliott, C. M.; Frank, A. J.; George, S. M. *J. Phys. Chem. C* **2010**, *114*, 8032–8039.

(13) Donsanti, F.; Weinberger, B.; Cowache, P.; Bernard, M. C.; Lincot, D. In *Mater. Res. Soc. Symp. Proc.* **2001**, *668*, H8.20.1−H8.20.8.
(14) Sterner, J.; Malmström, J.; Stolt, L. *Prog. Photovolt: Res. Appl.* **2005**, *13*, 179–193.
(15) Stuyven, G.; De Visschere, P.; Hikavyy, A.; Neyts, K. *J. Cryst. Growth* **2002**, *234*, 690–698.
(16) Kim, Y. S.; Yun, S. J. *Appl. Surf. Sci.* **2004**, *229*, 105–111.
(17) Tanskanen, J. T.; Bakke, J. R.; Pakkanen, T. A.; Bent, S. F. *J. Vac. Sci. Technol., A* **2011**, *29*, 031507.
(18) Bakke, J.; King, J.; Jung, H.; Sinclair, R.; Bent, S. *Thin Solid Films* **2010**, *518*, 5400–5408.
(19) Yousfi, E. B.; Fouache, J.; Lincot, D. *Appl. Surf. Sci.* **2000**, *153*, 223–234.
(20) Pankove, J. *Optical Processes in Semiconductors*; Dover: New York, 1975.
(21) Urbach, F. *Phys. Rev.* **1953**, *92*, 1324–1324.
(22) Nitsche, R. *J. Cryst. Growth* **1971**, *9*, 238–243.
(23) Lange, N. *Lange's Handbook of Chemistry*, 16th ed.; McGraw-Hill: New York, 2005.
(24) Yousfi, E. B.; Lincot, D. Study of Atomic Layer Epitaxy (ALE) of oxides (ZnO, Al2O3) and sulfides (ZnS, In2S3) thin films: In situ quartz crystal microgravimetry and application for Cu(In,Ga)Se2 solar cells. Thesis, Université Paris VI- Pierre et Marie Curie, Paris, 2000.
(25) Weast, R. C. *CRC Handbook of Chemistry and Physics*, 47th ed.; The Chemical Rubber Co.: Cleveland, OH, 1966.
(26) Yu, S.; Shu, L.; Wu, Y.; Yang, J.; Xie, Y.; Qian, Y. *J. Am. Ceram. Soc.* **1999**, *82*, 457–460.